How to cite: *Angew. Chem. Int. Ed.* **2024**, *63*, e202313315
doi.org/10.1002/anie.202313315

Supramolecular Chemistry

Magnetic Circular Dichroism Elucidates Molecular Interactions in Aggregated Chiral Organic Materials

Alessio Gabbani[+], *Andrea Taddeucci*[+], *Marco Bertuolo, Francesco Pineider, Laura Antonella Aronica, Lorenzo Di Bari, Gennaro Pescitelli, and Francesco Zinna**

Abstract: Chiral materials formed by aggregated organic compounds play a fundamental role in chiral optoelectronics, photonics and spintronics. Nonetheless, a precise understanding of the molecular interactions involved remains an open problem. Here we introduce magnetic circular dichroism (MCD) as a new tool to elucidate molecular interactions and structural parameters of a supramolecular system. A detailed analysis of MCD together with electronic circular dichroism spectra combined to ab initio calculations unveils essential information on the geometry and energy levels of a self-assembled thin film made of a carbazole di-bithiophene chiral molecule. This approach can be extended to a generality of chiral organic materials and can help rationalizing the fundamental interactions leading to supramolecular order. This in turn could enable a better understanding of structure–property relationships, resulting in a more efficient material design.

In recent years chiral conjugated molecules have extended the scope of functional materials and their applications in electronics.[1,2] Chiral semiconducting materials are used in the production and detection of circularly polarized (CP) light in CP-OLEDs[3–9] and CP-sensitive transistors.[10–14] Moreover, they can be employed to sort electrons by their spin through chirality induced spin selectivity (CISS).[15–18] Such properties are mainly controlled by the supramolecular structure in which the chiral compounds (small molecules, oligomers or polymers) assemble to give a supramolecular order upon thin film deposition.[19–25] Elucidating the geometry and structure of these materials is key to rationalize their behaviour and find structure–property relationships, which in turn could lead to rational design of new functional chiral materials.

Despite this, a precise understanding of the geometrical parameters of an aggregate at the molecular level is still non-trivial. In a chiral material, chirality can manifest itself at different hierarchical levels, from fibres (>1 μm) down to fibrils and bundles of fibrils (10–100 nm) and to supramolecular packing (1–10 nm).[1,26] Electron microscopies (AFM, SEM, TEM) are used to investigate structures with the sizes of fibrils or higher. On the other hand, chiroptical techniques such as natural electronic circular dichroism (ECD) can provide information at the molecular level, that is the first-order interactions between a molecule and its neighbours, but this technique, even coupled with ab initio calculations, is seldom conclusive. Indeed, calculations can corroborate a particular arrangement, but a purely computational approach may lead to several possible minimum energy structures, among which it is often impossible to reliably select one.[27] Therefore, finding a method to understand the first-order molecular interactions is still an open problem, which needs to be addressed to further advance the field of supramolecular chiral materials.

Another spectroscopic technique which employs CP light is magnetic circular dichroism (MCD). It exploits the property of all manner of chromophoric systems, both chiral and achiral, to preferentially absorb left or right CP light, when a sufficiently strong magnetic field is applied collinearly to the propagation direction of the light beam. MCD is mostly employed to characterize metal complexes,[28–32] semiconductors and perovskites,[33–36] plasmonic[37–42] and magnetic[43,44] nanoparticles and nanostructured inorganic materials,[45–49] etc. However, despite a few significant examples,[50–52] its role within the field of organic materials has yet to be established. MCD offers the advantage to be dominated by short range interactions, providing information about the pairing of a molecule with its close neighbours.[51] Once the molecular interaction modes are established, a bottom-up approach can in principle reveal structural features at a higher hierarchical level.

There are different molecular mechanisms giving rise to a MCD signal.[53–56] A common one is the selective absorption of left/right CP light by states that are split in the presence of a magnetic field due to Zeeman effect. However, this mechanism can play a role only when orbital or spin

[*] Dr. A. Gabbani,[+] A. Taddeucci,[+] M. Bertuolo, Prof. F. Pineider, Dr. L. A. Aronica, Prof. L. Di Bari, Prof. G. Pescitelli, Dr. F. Zinna
Dipartimento di Chimica e Chimica Industriale, Università di Pisa
Via Moruzzi 13, 56124 Pisa (Italy)
E-mail: francesco.zinna@unipi.it

Dr. A. Gabbani,[+] Prof. F. Pineider
Department of Physics and Astronomy, University of Florence
via Sansone 1, 50019 Sesto Fiorentino, FI (Italy)

A. Taddeucci[+]
Current affiliation: Diamond Light Source Ltd.
Fermi Avenue, Chilton, Didcot OX11 0DE (UK)

[+] These authors contributed equally to this work.

degenerate states exist in the system. Zeeman splitting of electronic states may occur only in the presence of a C_3 or higher rotation axis (for orbital degeneracy) or of unpaired spins (for spin degeneracy). Another mechanism, leading to MCD, is a field-induced mixing of excited states which are close in energy and mutually orthogonally polarized (see Figure 1 and Figure S6).[57] This is associated with the so-called Faraday's *B*-term (see below). Although weak MCD is usually obtained through *B*-term, in principle this mechanism is always at play regardless of the symmetry or spin properties of the compound.[55] Given the low symmetry of the system investigated here, the *B*-term is the only one relevant to describe all the observed MCD features.

In this work we show how MCD, together with ECD and ab initio calculations, may be used to gain information about the molecular interactions and structural features at the base of supramolecular assemblies within a thin film of a conjugated chiral organic compound.

To demonstrate the potential of this approach, we chose a di-bithiophene derivative of carbazole. A chiral chain derived from citronellol is introduced on the carbazole N-atom. The structure of the compound is shown in Scheme 1 (**Th-CBZ** = *(S)*-3,6-di([2,2′-bithiophen]-5-yl)-9-(3,7-dimethyloctyl)-9H-carbazole). Such molecule is representative of a widely investigated class of compounds, featuring an aromatic core, one or more chiral alkyl chains and conjugated moieties, such as thiophene groups.[1,4,58] These compounds are known to undergo aggregation and form supramolecular chiral assemblies, often showing exciton interactions (Figure 1). These systems are also investigated for special applications in electronics and photonics.[4,59,60]

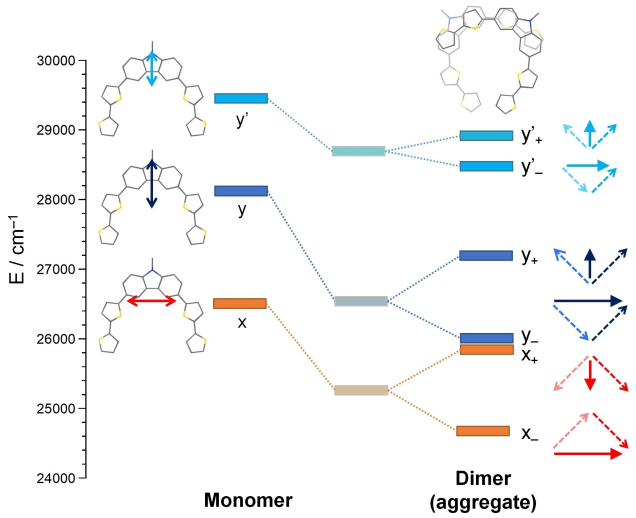

Figure 1. Experimental energy levels of the excited states of the monomer and aggregate (dimer) of **Th-CBZ** extracted by fitting MCD spectra. The direction of transition dipoles shown on the left side (full double arrows) is obtained from TD-DFT calculations, that on the right side represent the in-phase and out-of-phase combinations (full arrows) of monomer transition dipoles (dashed arrows).

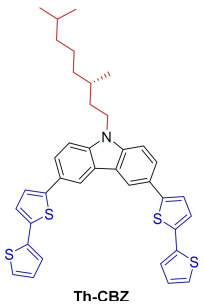

Scheme 1. **Th-CBZ** molecular structure.

As is the case for similar molecules,[1,4,58] **Th-CBZ** does not show any ECD in CH_2Cl_2 solution, since the stereogenic centre in the chiral aliphatic chain is not sufficient to induce any significant rotatory strength on the transitions of the conjugated core of single, isolated molecules (Figure 2d). The absence of aggregation in CH_2Cl_2 solution is observed at least up to 10^{-3} M concentration (Figure S4). Upon thin film deposition by spin coating, the sample is still ECD-silent (Figure 2e), but after exposing the film to dichloromethane vapours for a few minutes (solvent annealing), an intense (absorption dissymmetry factor, $g_{abs} = -0.02$ at 426 nm) negative couplet structure arises centred at 380 nm (Figure 2f). This indicates that the material has reached a stereochemically ordered aggregation mode.

Unlike in ECD, under an external magnetic field of 1.4 T we observed a weak but significant MCD for **Th-CBZ** in dichloromethane solution associated to the main absorption band centred at 370 nm. The magnetic field (H) normalized dissymmetry factor, $g_{MCD} = \frac{\Delta A}{A} \cdot \frac{1}{H}$, is approximately $5 \cdot 10^{-5}$ T^{-1}, of the same order as those observed for other simple aromatic molecules.[52,61–64] In the 320–500 nm region, the MCD spectrum consists of 3 bands of alternating sign, with a prominent negative feature at 390 nm. TD-DFT calculations (CAM-B3LYP/def2-TZVP level) show that the main absorption band for the monomer (450–320 nm, Figure S1) is composed of 3 electronic transitions (Table S5 and Figure 1). It must be stressed that the chromophoric unit in **Th-CBZ** is not planar because of the deviations of the inter-aryl junctions from planarity; ideally it may adopt two limiting symmetries: C_s (vertical symmetry plane) or C_2, depending on the relative twist of the two junctions, but several different conformers with variable inter-aryl torsions are possible (see Supporting Information). Given the similarity of the electronic levels in the two conformers, for the sake of simplicity, the following discussion is focused on the C_s-symmetric one (optimized at B3LYP-D3BJ/6-31+G(d) level). The lowest energy transition is polarized along the *x*-axis of the molecule, while the other two are polarized along the *y*-axis (see Figure 1). The U-shape of the molecule assures that y- and x-polarized transitions are close in energy, which is necessary to give a non-negligible MCD signal. In the following, we refer to these transitions as **x**, **y** and **y'**. As discussed above, in closed-shell, low molecular symmetry compound, as in C_s- or C_2, magnetooptical activity can originate only from the Faraday *B*-term. The main term describing the MCD transition associated with **x** state is:

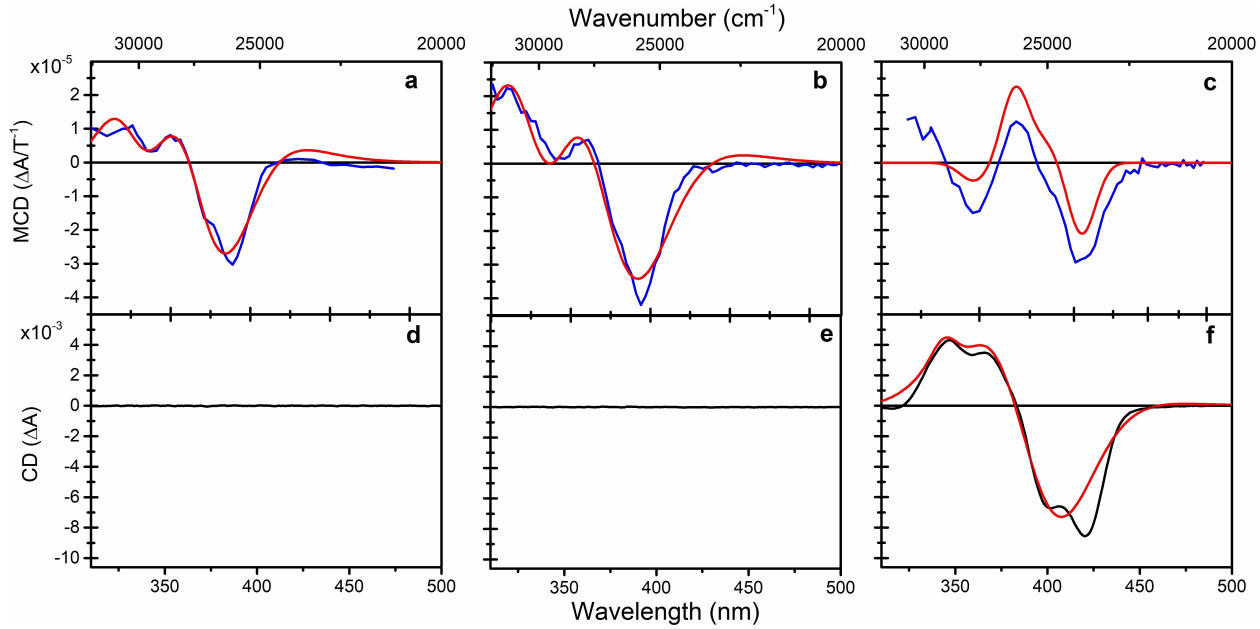

Figure 2. MCD and ECD spectra of *(S)*-**Th-CBZ** in solution (a, d), in the as-cast film (b, e) and in the annealed film (c, f). The red curves represent the best fits according to the models discussed in the text.

$$B_x = Im\left\{\frac{\mathbf{m}_{xy}\cdot(\boldsymbol{\mu}_x\times\boldsymbol{\mu}_y)}{E_y-E_x}+\frac{\mathbf{m}_{xy'}\cdot(\boldsymbol{\mu}_x\times\boldsymbol{\mu}_{y'})}{E_{y'}-E_x}\right\} \quad (1)$$

where $\boldsymbol{\mu}_x$, $\boldsymbol{\mu}_y$ and $\boldsymbol{\mu}_{y'}$ are the electric transition dipoles from the ground state and $\mathbf{m}_{xy}$ and $\mathbf{m}_{xy'}$ are the magnetic transition dipoles between the excited states of energy E_x, E_y and $E_{y'}$. Similar expressions can be written (see SI, eq. S2–S4) for the transitions to **y** and **y'** state (B_y and $B_{y'}$), so in total 3 MCD bands are expected. This is in agreement with the experimental data, as the experimental MCD spectrum can be satisfactorily fitted with this model (see eq. S5), where the 3 normalized Gaussian functions are weighed by the above-mentioned expression for B_x, B_y and $B_{y'}$ (Figure 2a). The energies of the 3 states as determined by TD-DFT calculations were used, with a systematic correction established by the fitting ($-1715\,cm^{-1}$, see Table S1 and S5), due to the known overestimation of transition energies by CAM-B3LYP functional.[65]

Upon thin-film deposition, a MCD spectrum almost identical to the solution one (except for a slight red shift) is obtained. This is in agreement with the fact that the as-cast film features randomly oriented molecules, in a similar situation as in solution. The red shift is likely to be related to some planarization occurring in the (disordered) solid state, associated with the fact that the energy barrier toward planarization is small ($<1\,kcal\,mol^{-1}$).[66] Again, the same formula used for the compound in solution can be applied to fit the MCD spectrum of the as-cast film (Figure 2b).

Interestingly, after solvent annealing the MCD spectrum of the film is completely different, similar to what happens for ECD, signalling again that some supramolecular order has been reached (Figure 2c). In particular, the MCD shows a more complex pattern of bands of alternating sign. In order to rationalize such features and to gain insight into the structural motif giving rise to the observed MCD spectrum, we propose the following treatment of the experimental data.

We rationalize the MCD spectrum by means of an exciton-like model, by taking into account dimeric pairs,[52,68–70] with the purpose of extracting geometrical quantitative information about the molecular interaction modes from the spectral signature and shape. Although we expect the effective molecular aggregate to be much larger, the use of a dimeric model is justified by the special sensitivity of MCD to the local environment, being its response dominated by short range interactions.[51]

A full quantitative model describing the MCD of interacting molecules is not yet available; however, a simplified exciton model for MCD was recently proposed by Lakhwani et al. in the case of pentacene dimers.[52] This model considers degenerate coupling within the framework of a dipolar approximation. We can consider a **Th-CBZ** dimer, where each of the 3 excited state levels of the monomer (**x**, **y**, **y'**) is split into 2 components ($\mathbf{x}_{\pm}$, $\mathbf{y}_{\pm}$, $\mathbf{y'}_{\pm}$) due to dipolar/exciton interaction (Figure 1). These 6 levels undergo magnetic field-induced mixing according to their polarization, giving rise to exciton *B*-terms. Such interactions depend on the Euler angles describing the relative orientations of the monomer units in the dimer. We assume that mainly co-facial interactions due to stacking are present (with no significant edge-to-face contributions). Thus, the expressions for *B*-terms, gauging the intensity of each transition and therefore the shape of the overall MCD spectrum, are greatly simplified. This simplification occurs because of the excitonic origin of the considered transitions and the orthogonal arrangement between the component monomer transitions (**x** *vs* **y**/**y'**), as well as on their excitonic combinations (Figure 1). In this situation, *B*-terms depend only on one angle (α,

Figure 3a), which describes the rotation of one monomer with respect to the other around the *z*-axis, perpendicular to the carbazole plane. In other words, *pitch* and *roll* inclinations are assumed to be negligibly small with respect to the rotation angle α around the z-axis (*yaw*).[67] The Faraday *B*-term associated with each transition depends on the monomer-centered magnetic/electric transitions ($m\mu\mu$ terms), the energy of each level, as well as on the angle α. By adapting Lakhwani's formulae[52] to the case of 3 interacting excited states, the *B*-term becomes (for the transition to the $\mathbf{x}_-$ level):

$$B_{x_-} = \frac{1}{4} m_{xy} \mu_x \mu_y \frac{2 - 2\cos\alpha}{E_{x_-} - E_{y_-}} + \frac{1}{4} m_{xy'} \mu_x \mu_{y'} \frac{2 - 2\cos\alpha}{E_{x_-} - E_{y'_-}} \quad (2)$$

where the other mixing terms (e.g., $\mathbf{x}_-$ with $\mathbf{y}_+$) are null. Similar expressions can be written for the *B*-terms of all the 6 states (B_{x_-}, B_{x_+}, B_{y_-}, B_{y_+}, $B_{y'_-}$ $B_{y'_+}$) and are reported in the Supporting Information (eq. S13–S18). The experimental MCD spectrum is therefore fitted with Gaussian functions by using the expressions above for the *B*-terms as the weights (see Figure 2c and eq. S19). Despite the simplicity of the model, the analysis provides a good agreement with the experimental data for most of the spectral region. The lack of agreement in the region above 29000 cm^{-1} is due to the fact that the high energy $\mathbf{y'}_+$ state can mix with higher energy transitions not included in our treatment. In this way, the angle α is obtained as a fitting parameter directly from the experimental MCD spectrum, as well as the energy levels (Figure 1 and Table S2), and therefore the exciton coupling potentials. The best fit is obtained for an angle of approximately 90° (87 ±1 0°). The strong dependence of the MCD shape as a function of the angle can be appreciated by simulating the spectrum according to equation S19 for different α values (Figure 3b). It should be noticed that only the absolute value of the angle α can be recovered through the above-mentioned procedure, as MCD by itself is not sensitive to the dimer handedness, i.e. to the specific enantiomer measured. The sign of the angle (−90° for *(S)*-**Th-CBZ**) can be extracted from the sign of the exciton coupling (negative) of the ECD spectrum. Taking this information into account, we could build a model of the dimeric structure, as shown in Figure 3a.

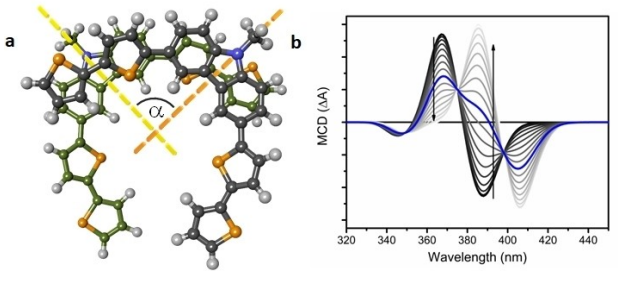

Figure 3. Truncated dimeric model constructed using the information extracted from the MCD/ECD spectra, α=-90° (a). Simulated MCD spectrum according to equation S19 for |α| ranging from 0° to 180° in 10° steps; arrows direction indicates increasing α values; the spectrum obtained for |α| =90° is highlighted in blue (b).

The same energies found for the MCD can be employed to fit the ECD spectrum (Figure 2f). Again, within the framework of a dimer interaction, exciton rotatory strengths ($R_{x_\pm}$, $R_{y_\pm}$, $R_{y'_\pm}$) can be written as:[71,72]

$$R_{x_\pm} = \pm\frac{1}{2}\left(E_{x_+} - E_{x_-}\right)\mathbf{r}_{12} \cdot \left(\boldsymbol{\mu}_{1,x} \times \boldsymbol{\mu}_{2,x}\right) \quad (3)$$

where $\mu_{1,x}/\mu_{2,x}$ are the electric transition dipole moments associated to the **x** state for the first and second monomer of the dimer and $\mathbf{r}_{12}$ is the distance between them (see the Supporting Information for $R_{y_\pm}$, $R_{y'_\pm}$expressions). Only degenerate coupling is considered because non-degenerate coupling, e.g. between **x** and **y** transitions, is intrinsically weaker[73,74] and may be safely neglected here because these transitions lie parallel to each other for the assumed geometry (see Figure 1). For fitting the ECD, μ values are taken from TD-DFT calculations of the monomer (Table S5), while the energies are the ones determined through the MCD fitting. The rotatory strengths are again convoluted with Gaussian functions (eq. S23).

The quality of the fittings obtained for both MCD and ECD shows that the exciton approach used herein is, within its approximations, suitable to semi-quantitatively describe the interaction and the resulting spectral features.

The geometrical parameters extracted from the MCD spectrum can be used as constraints for ab initio calculations on a dimeric structure. A truncated dimer (where the alkyl chains were replaced with methyl groups) consisting of two monomers stacked at 3.6 Å plane-to-plane distance and rotated by −90° with respect to each other was built (Figure 3a). No horizontal translation of one monomer with respect to the other was necessary, as the stacking interactions are maximized when the molecules are rotated around the same axis perpendicular to the carbazole planes (as in Figure 3). On this structure, TD-CAM-B3LYP/def2-TZVP calculations were carried out. The first 6 excited state energies obtained from TD-DFT satisfactorily agree with the energies of the exciton levels experimentally found from the spectral fitting (Figure S17), apart from a systematic overestimation. Natural transition orbital analysis[75,76] confirms the dominant excitonic nature of these states (Figure S18). Moreover, the computed rotatory strengths associated to such energies also provide a reasonable match with the experimental ECD spectrum (Figures S19). We note anyway that the ECD may be heavily affected by longer range interactions, beyond the dimer considered for the TD-DFT calculations. On the other hand, MCD is expected to be less significantly influenced by non-neighbouring molecular units.[51] Moreover, we are neglecting vibronic couplings which may alter the spectral shapes.[77]

For completeness, the higher hierarchical level of aggregation was investigated by means of optical, atomic force (AFM) and field effect scanning electron microscopy (FE-SEM). FE-SEM shows a surface with a wavy-wrinkling texture on the μm scale for the as-cast film (Figure S9). On the other hand, for the thermally annealed film, both FE-SEM and AFM reveal the presence of right-handed helical fibrils at the mesoscale domain (Figure S10–S14) lying on the

plane of the glass surface. AFM images show fibrils with a diameter estimated approximately 5–10 nm covering the surface uniformly. The main axes of the fibrils are randomly oriented on the plane. This fact, together with the chromophore in-plane polarization of the major transitions, makes the emergent chiroptical signals isotropic. The presence of larger bundles (approx. 50 nm) is also observed in both FE-SEM and AFM images. The size of the smaller fibrils (5–10 nm) is compatible with a bundle of approximately 4 columnar aggregates of **Th-CBZ**, formed by repeating the 90° pairwise stacking interaction elucidated above (Figure S20). Larger fibrils may be formed by more columnar aggregates packed together. As it was pointed out in many instances, the handedness found at higher hierarchical levels is not necessarily related to the handedness of the molecular interactions in a simple way.[1] The optical microscopy images (Figure S8) suggest the absence of domains or phase separations on the 100/1000 μm scale. Finally, we note that the supramolecular assembly is not thickness-dependent in the investigated range (60–280 nm), as both ECD and MCD intensity scale linearly with the film thickness (Figure S5).

In conclusion, we showed how critical geometrical parameters leading to supramolecular structures in chiral organic materials can be obtained from MCD data. This approach is based on a relatively simple protocol which could be applied in a generality of cases, to a vast number of chiral supramolecular assemblies and packing modes of small conjugated molecules or even polymers. The addition of magnetooptical techniques to already established methods to elucidate molecular interactions in aggregates could lead to a deeper understanding of structure-function relationships and help chemists and materials scientists to develop more performant chiral functional materials, for applications ranging from chiral photonics to chiral electronics and spintronics.

Supporting Information

The authors have cited additional references within the Supporting Information.[52,58,78]

Acknowledgements

The authors thank CISUP—Centre for Instrumentation Sharing—University of Pisa, for FE-SEM (Dr. Randa Anis Ishak) and AFM (Dr. Michele Alderighi) analysis. G. P. gratefully acknowledges the University of Pisa for the availability of high-performance computing resources and support through the service computing@unipi. Dr. Lorenzo Cupellini (University of Pisa) is thanked for stimulating discussions. A.G. and F.P. acknowledge the financial support of PRIN2017 under Grant No. 2017CR5WCH Q-ChiSS (Italian MIUR).

Conflict of Interest

The authors declare no conflict of interest.

Data Availability Statement

The data that support the findings of this study are available from the corresponding author upon reasonable request.

Keywords: Chirality · Exciton Interactions · Magnetic Circular Dichroism · Self-Assembly · Thin Films

[1] G. Albano, G. Pescitelli, L. Di Bari, *Chem. Rev.* **2020**, *120*, 10145–10243.
[2] J. Crassous, M. J. Fuchter, D. E. Freedman, N. A. Kotov, J. Moon, M. C. Beard, S. Feldmann, *Nat. Rev. Mater.* **2023**, *8*, 365–371.
[3] Y. Zhang, T. Jing, Y. Quan, S. Ye, Y. Cheng, *Adv. Opt. Mater.* **2022**, *10*, 2200915.
[4] G. Albano, L. A. Aronica, A. Minotto, F. Cacialli, L. Di Bari, *Chem. Eur. J.* **2020**, *26*, 16622–16627.
[5] L. Wan, Y. Liu, M. J. Fuchter, B. Yan, *Nat. Photonics* **2023**, *17*, 193–199.
[6] L. Wan, J. Wade, X. Shi, S. Xu, M. J. Fuchter, A. J. Campbell, *ACS Appl. Mater. Interfaces* **2020**, *12*, 39471–39478.
[7] X. Zhang, Z. Xu, Y. Zhang, Y. Quan, Y. Cheng, *J. Mater. Chem. C* **2020**, *8*, 15669–15676.
[8] Y. Yang, R. C. da Costa, D.-M. Smilgies, A. J. Campbell, M. J. Fuchter, *Adv. Mater.* **2013**, *25*, 2624–2628.
[9] L. Wan, J. Wade, F. Salerno, O. Arteaga, B. Laidlaw, X. Wang, T. Penfold, M. J. Fuchter, A. J. Campbell, *ACS Nano* **2019**, *13*, 8099–8105.
[10] Y. Yang, R. C. da Costa, M. J. Fuchter, A. J. Campbell, *Nat. Photonics* **2013**, *7*, 634–638.
[11] J. Cheng, F. Ge, C. Zhang, Y. Kuai, P. Hou, Y. Xiang, D. Zhang, L. Qiu, Q. Zhang, G. Zou, *J. Mater. Chem. C* **2020**, *8*, 9271–9275.
[12] C. Zhang, X. Wang, L. Qiu, *Front. Chem.* **2021**, *9*, 711488.
[13] L. Zhang, J. Ahn, M. Han, M. Linares, M. Surin, H.-J. Zhang, J. H. Oh, J. Lin, *Nat. Commun.* **2021**, *12*, 142.
[14] W. Shi, F. Salerno, M. D. Ward, A. Santana-Bonilla, J. Wade, X. Hou, T. Liu, T. J. S. Dennis, A. J. Campbell, K. E. Jelfs, M. J. Fuchter, *Adv. Mater.* **2021**, *33*, 2004115.
[15] V. Kiran, S. P. Mathew, S. R. Cohen, I. Hernández Delgado, J. Lacour, R. Naaman, *Adv. Mater.* **2016**, *28*, 1957–1962.
[16] P. C. Mondal, N. Kantor-Uriel, S. P. Mathew, F. Tassinari, C. Fontanesi, R. Naaman, *Adv. Mater.* **2015**, *27*, 1924–1927.
[17] R. Rodríguez, C. Naranjo A Kumar, P. Matozzo, T. K. Das, Q. Zhu, N. Vanthuyne, R. Goméz, R. Naaman, L. Sánchez, J. Crassous, *J. Am. Chem. Soc.* **2022**, *144*, 7709–7719.
[18] A. Privitera, E. Macaluso, A. Chiesa, A. Gabbani, D. Faccio, D. Giuri, M. Briganti, N. Giaconi, F. Santanni, N. Jarmouni, L. Poggini, M. Mannini, M. Chiesa, C. Tomasini, F. Pineider, E. Salvadori, S. Carretta, R. Sessoli, *Chem. Sci.* **2022**, *13*, 12208–12218.
[19] Y. Yang, B. Rice, X. Shi, J. R. Brandt, R. C. da Costa, G. J. Hedley, D.-M. Smilgies, J. M. Frost, I. D. W. Samuel, A. Otero-de-la-Roza, E. R. Johnson, K. E. Jelfs, J. Nelson, A. J. Campbell, M. J. Fuchter, *ACS Nano* **2017**, *11*, 8329–8338.
[20] J. Wade, J. N. Hilfiker, J. R. Brandt, L. Liirò-Peluso, L. Wan, X. Shi, F. Salerno, S. T. J. Ryan, S. Schöche, O. Arteaga, T. Jávorfi, G. Siligardi, C. Wang, D. B. Amabilino, P. H. Beton, A. J. Campbell, M. J. Fuchter, *Nat. Commun.* **2020**, *11*, 6137.
[21] B. Laidlaw, J. Eng, J. Wade, X. Shi, F. Salerno, M. J. Fuchter, T. J. Penfold, *Chem. Commun.* **2021**, *57*, 9914–9917.
[22] J. L. Greenfield, J. Wade, J. R. Brandt, X. Shi, T. J. Penfold, M. J. Fuchter, *Chem. Sci.* **2021**, *12*, 8589–8602.
[23] G. Albano, A. Taddeucci, G. Pescitelli, L. Di Bari, *Chem. Eur. J.* **2023**, *29*, e202301982.

[24] J. Wade, J. R. Brandt, D. Reger, F. Zinna, K. Y. Amsharov, N. Jux, D. L. Andrews, M. J. Fuchter, *Angew. Chem. Int. Ed.* **2021**, *60*, 222–227.
[25] J. Wade, F. Salerno, R. C. Kilbride, D. K. Kim, J. A. Schmidt, J. A. Smith, L. M. LeBlanc, E. H. Wolpert, A. A. Adeleke, E. R. Johnson, J. Nelson, T. Mori, K. E. Jelfs, S. Heutz, M. J. Fuchter, *Nat. Chem.* **2022**, *14*, 1383–1389.
[26] S. M. Morrow, A. J. Bissette, S. P. Fletcher, *Nat. Nanotechnol.* **2017**, *12*, 410–419.
[27] W. Tang, Q. Zhou, *Phys. Rev. E* **2012**, *86*, 031909.
[28] J. Mack, Y. Asano, N. Kobayashi, M. J. Stillman, *J. Am. Chem. Soc.* **2005**, *127*, 17697–17711.
[29] M. Sundararajan, D. Ganyushin, S. Ye, F. Neese, *Dalton Trans.* **2009**, 6021–6036.
[30] A. Westphal, A. Klinkebiel, H.-M. Berends, H. Broda, P. Kurz, F. Tuczek, *Inorg. Chem.* **2013**, *52*, 2372–2387.
[31] V. E. Fleischauer, G. Ganguly, D. H. Woen, N. J. Wolford, W. J. Evans, J. Autschbach, M. L. Neidig, *Organometallics* **2019**, *38*, 3124–3131.
[32] N. J. Wolford, X. Yu, S. C. Bart, J. Autschbach, M. L. Neidig, *Dalton Trans.* **2020**, *49*, 14401–14410.
[33] C. Stamper, R. P. Sabatini, S. Bernardi, C. Liao, E. Dennis, A. Sharma, A. Widmer-Cooper, M. I. Saidaminov, A. W. Y. Ho-Bailie, G. Lakhwani, *Chirality* **2021**, *33*, 610–617.
[34] S. Dutta, L. Yang, S. Y. Liu, C. M. Liu, L. J. Liaw, S. Som, A. Mohapatra, R. Sankar, W. C. Lin, Y. C. Chao, *Mater. Today Phys.* **2022**, *27*, 100843.
[35] R. Pan, S. Tao, K. Wang, Z.-G. Yu, *Chem. Mater.* **2023**, *35*, 1667–1673.
[36] M. Kuno, M. Nirmal, M. G. Bawendi, A. Efros, M. Rosen, *J. Chem. Phys.* **1998**, *108*, 4242–4247.
[37] A. Gabbani, G. Petrucci, F. Pineider, *J. Appl. Phys.* **2021**, *129*, 211101.
[38] A. Gabbani, G. Campo, V. Bonanni, P. van Rhee, G. Bottaro, C. de Julián Fernández, V. Bello, E. Fantechi, F. Biccari, M. Gurioli, L. Armelao, C. Sangregorio, G. Mattei, P. Christiansen, F. Pineider, *J. Phys. Chem. C* **2022**, *126*, 1939–1945.
[39] B. Han, X. Gao, J. Lv, Z. Tang, *Adv. Mater.* **2020**, *32*, 1801491.
[40] A. Gabbani, C. Sangregorio, B. Tandon, A. Nag, M. Gurioli, F. Pineider, *Nano Lett.* **2022**, *22*, 9036–9044.
[41] P. Yin, H. Fang, M. Hegde, P. V. Radovanovic, *Nat. Nanotechnol.* **2018**, *13*, 463–467.
[42] K. H. Hartstein, A. M. Schimpf, M. Salvador, D. R. Gamelin, *J. Phys. Chem. Lett.* **2017**, *8*, 1831–1836.
[43] G. Campo, F. Pineider, V. Bonanni, M. Albino, A. Caneschi, C. de Julián Fernández, C. Innocenti, C. Sangregorio, *Chem. Mater.* **2015**, *27*, 466–473.
[44] E. Fantechi, C. Innocenti, G. Bertoni, C. Sangregorio, F. Pineider, *Nano Res.* **2020**, *13*, 785–794.
[45] G. Petrucci, A. Gabbani, I. Faniayeu, E. Pedrueza-Villalmanzo, G. Cucinotta, M. Atzori, A. Dmitriev, F. Pineider, *Appl. Phys. Lett.* **2021**, *118*, 251108.
[46] J. Kuttruff, A. Gabbani, G. Petrucci, Y. Zhao, M. Iarossi, E. Pedrueza-Villalmanzo, A. Dmitriev, A. Parracino, G. Strangi, F. De Angelis, D. Brida, F. Pineider, N. Maccaferri, *Phys. Rev. Lett.* **2021**, *127*, 217402.
[47] G. Varvaro, A. Di Trolio, A. Polimeni, A. Gabbani, F. Pineider, C. de Julián Fernández, G. Barucca, P. Mengucci, A. Amore Bonapasta, A. M. Testa, *J. Mater. Chem. C* **2019**, *7*, 78–85.
[48] N. Maccaferri, A. Berger, S. Bonetti, V. Bonanni, M. Kataja, Q. H. Qin, S. van Dijken, Z. Pirzadeh, A. Dmitriev, J. Nogués, J. Åkermann, P. Vavassori, *Phys. Rev. Lett.* **2013**, *111*, 167401.
[49] A. López-Ortega, M. Zapata-Herrera, N. Maccaferri, M. Pancaldi, M. Garcia, A. Chuvilin, P. Vavassori, *Light-Sci. Appl.* **2020**, *9*, 49.
[50] Y. Kitagawa, H. Segawa, K. Ishii, *Angew. Chem. Int. Ed.* **2011**, *50*, 9133–9136.
[51] A. Sharma, J. P. Wojciechowski, Y. Liu, T. Pelras, C. M. Wallace, M. Müllner, A. Widmer-Cooper, P. Thordarson, G. Lakhwani, *Cell Rep. Phys. Sci.* **2020**, *1*, 100148.
[52] A. Sharma, S. Athanasopoulos, Y. Li, S. N. Sanders, E. Kumarasamy, L. M. Campos, G. Lakhwani, *J. Phys. Chem. Lett.* **2022**, *13*, 8978–8986.
[53] P. J. Stephens, *J. Chem. Phys.* **1970**, *52*, 3489–3516.
[54] W. R. Mason, Magnetic circular dichroism spectroscopy, John Wiley & Sons, Hoboken, **2007**.
[55] Z. Nelson, L. Delage-Laurin, T. M. Swager, *J. Am. Chem. Soc.* **2022**, *144*, 11912–11926.
[56] F. Zinna, G. Pescitelli, *Eur. J. Org. Chem.* **2023**, e202300509.
[57] J. Mack, M. J. Stillman, N. Kobayashi, *Coord. Chem. Rev.* **2007**, *251*, 429–453.
[58] G. Albano, F. Salerno, L. Portus, W. Porzio, L. A. Aronica, L. Di Bari, *ChemNanoMat* **2018**, *4*, 1059–1070.
[59] N. Y. Kim, J. Kyhm, H. Han, S. J. Kim, J. Ahn, D. K. Hwang, H. W. Jang, B.-K. Ju, J. A. Lim, *Adv. Funct. Mater.* **2019**, *29*, 1808668.
[60] K. Wang, Y. Xiao, *Chirality* **2021**, *33*, 424–446.
[61] C. Djerassi, E. Bunnenberg, D. L. Elder, *Pure Appl. Chem.* **1971**, *25*, 57–90.
[62] M. Vasak, M. R. Whipple, A. Berg, J. Michl, *J. Am. Chem. Soc.* **1978**, *100*, 6872–6877.
[63] M. R. Whipple, M. Vasak, J. Michl, *J. Am. Chem. Soc.* **1978**, *100*, 6844–6852.
[64] A. Tajiri, J. Winkler, *Z. Naturforsch.* **1983**, *38*, 1263–1269.
[65] D. Jacquemin, V. Wathelet, E. A. Perpète, C. Adamo, *J. Chem. Theory Comput.* **2009**, *5*, 2420–2435.
[66] J. B. Lin, Y. Jin, S. A. Lopez, N. Druckerman, S. E. Wheeler, K. N. Houk, *J. Chem. Theory Comput.* **2017**, *13*, 5624–5638.
[67] G. Gryn'ova, A. Nicolaï, A. Prlj, P. Ollitrault, D. Andrienko, C. Corminboeuf, *J. Mater. Chem. C* **2017**, *5*, 350–361.
[68] D. Zevenhuijzen, P. J. Zandstra, *Biophys. Chem.* **1984**, *19*, 121–129.
[69] J. L. Hughes, R. Razeghifard, M. Logue, A. Oakley, T. Wydrzynski, E. Krausz, *J. Am. Chem. Soc.* **2006**, *128*, 3649–3658.
[70] J. L. Hughes, R. J. Pace, E. Krausz, *Chem. Phys. Lett.* **2004**, *385*, 116–121.
[71] G. Pescitelli, *Chirality* **2022**, *34*, 333–363.
[72] N. Harada, K. Nakanishi, *Circular Dichroic Spectroscopy - Exciton Coupling in Organic Stereochemistry*, University Science Books, Mill Valley, CA, USA, **1983**.
[73] G. Pescitelli, L. Di Bari, *Chirality* **2017**, *29*, 476–485.
[74] P. L. Polavarapu, *Chiroptical Spectroscopy: Fundamentals and Applications*, FL: CRC Press, Boca Raton, FL, USA, **2016**.
[75] R. L. Martin, *J. Chem. Phys.* **2003**, *118*, 4775–4777.
[76] T. Lu, F. Chen, *J. Comput. Chem.* **2012**, *33*, 580–592.
[77] D. Padula, F. Santoro, G. Pescitelli, *RSC Adv.* **2016**, *6*, 37938–37943.
[78] J. Li, Y. Chen, C. Yang, W.-Y. Lai, *Synlett* **2015**, *26*, 2451–2456.

Manuscript received: September 7, 2023
Accepted manuscript online: November 14, 2023
Version of record online: November 29, 2023